Hydration of Cm^{3+} in Aqueous Solution from 20 to 200 °C. A Time-Resolved Laser Fluorescence Spectroscopy Study

Patric Lindqvist-Reis,* Reinhardt Klenze, Günther Schubert, and Thomas Fanghänel

Institut für Nukleare Entsorgung, Forschungszentrum Karlsruhe, P.O. Box 3640, 76021 Karlsruhe, Germany

Received: October 1, 2004; In Final Form: November 24, 2004

Time-resolved laser fluorescence spectroscopy (TRLFS) is used to study the hydration of the Cm^{3+} ion in acidified (0.1 M perchloric acid) H_2O and D_2O from 20 to 200 °C. Strong temperature dependency is found for several of the spectroscopic quantities associated with the $^6D'_{7/2} \rightarrow {}^8S'_{7/2}$ photoemission spectra, with similar relative changes in both solvents. The emission band shifts to lower energy with increasing temperature, which is attributed to an equilibrium between hydrated Cm^{3+} ions with different numbers of water molecules in the first coordination sphere, namely $[Cm(H_2O)_9]^{3+}$ and $[Cm(H_2O)_8]^{3+}$. Comparison with crystalline reference compounds and the analysis of hot bands corroborates the assignment of these species. The molar fraction of the octahydrated species increases from ∼10% at room temperature to ∼40% at 200 °C, indicating an entropy driven reaction. The corresponding thermodynamic parameters are obtained as $\Delta H° = +13.1 \pm 0.4$ kJ mol^{-1}, $\Delta S° = +25.4 \pm 1.2$ J mol^{-1} K^{-1}, and $\Delta G^{298} = +5.5 \pm 0.6$ kJ mol^{-1}. Both the emission intensity and lifetime decrease with increasing temperature. The temperature dependency of the nonradiative decay rate of the emitting $^6D'_{7/2}$ level follows an Arrhenius equation with the activation energy 26.5 kJ mol^{-1} (2250 cm^{-1}) in both H_2O and D_2O, which is somewhat lower than the energy gap between $^6D'_{7/2}$ and $^6P'_{5/2}$ exited state levels.

1. Introduction

Notable progress has been achieved in recent years to establish a thermodynamic database for lanthanides and actinides in aquatic systems.[1] The collected data enables quantification of the geochemical behavior of these elements in the geosphere, which is of particular importance for the long-term prediction of the migration of actinides from a nuclear waste repository. However, while the present data almost exclusively are restricted to ambient temperature, modeling of certain chemical reactions at elevated temperature, e.g., rare earth hydrothermal ore deposition and reactions of actinides in nuclear waste repositories, is very limited. In the repository scenario, depending on the waste loading and the type of geoengineered barrier, the temperature at the canister surface may be increased up to 200 °C due to radioactive decay.

In an aqueous electrolyte solution at elevated temperature the hydrogen bond network of water is partially broken. This reduces the screening between ions and thereby increases the tendency for ion-pair formation. Theoretical calculations of complexation of trivalent lanthanide (Ln^{3+}) ions with common ligands such as OH^-, Cl^-, and NO_3^- in aqueous solution at elevated temperature and pressure have confirmed this general picture,[2] while detailed knowledge of the ion−water interaction and the structure of the Ln^{3+} aqua complex under such conditions is rather poor. In contrast, the structure and dynamic properties of these aqua ions at ambient temperature are well documented,[3] while less is known about the structure of the trivalent actinide (An^{3+}) aqua ions. Nevertheless, Ln^{3+} and An^{3+} aqua ions of similar ionic radii are expected to have similar structures and dynamic properties.[4−6] In accordance with the lanthanide series, where ions in the beginning and the end of the series exclusively occur as nona- and octahydrates, respectively, a similar trend is expected for the actinides. Based on ionic radii and comparison with Ln^{3+} data, it has been suggested that the hydration number changes from nine to eight between Cm^{3+} and Es^{3+},[5−7] implying an equilibrium between nona- and octahydrated species

$$[An(H_2O)_9]^{3+} \rightleftharpoons [An(H_2O)_8]^{3+} + H_2O \qquad (1)$$

The decrease in the Ln^{3+} ionic radii across the series is well-reproduced in experiments (e.g., X-ray diffraction and EXAFS), showing an equal decrease in the mean Ln−O bond distance of the aqua ions. Indeed, the hydration numbers for the intermediate Sm^{3+} and Eu^{3+} ions were found to be near 8.5 from X-ray and neutron diffraction at ambient temperature.[8,9] A molecular dynamic simulation resulted in hydration numbers of 9, 8.5, and 8 for Nd^{3+}, Sm^{3+}, and Yb^{3+}, respectively,[10] whereas hydration number 9 was obtained for Nd^{3+}, Gd^{3+}, and Yb^{3+} in a similar study.[11] EXAFS has been used to derive coordination numbers and distances of the first hydration sphere for the U^{3+}−Cf^{3+} aqua ions at ambient temperature.[12−20] The results show a decrease in the An−O distance with increasing atomic number as expected, whereas the obtained coordination numbers are scattered between about 7 and 10. In a recent EXAFS study on aqueous Cm^{3+} solution it is shown that the Cm−O bond distance and coordination number are strongly dependent on the structure model applied.[21a]

As noted above, there are rather few spectroscopic studies on the structure of hydrated Ln^{3+} ions and their complexes in aqueous solution at elevated temperature. To our knowledge no such studies have been carried out for An^{3+} ions. An UV−vis spectroscopy study has recently been performed on the Nd^{3+} chloride complexation up to 250 °C,[22] and EXAFS has been used to study the local structure of La^{3+} in dilute HNO_3 up to

* Address correspondence to this author. Phone: +49-724-7822389. Fax: +49-724-7823927. E-mail: plr@ine.fzk.de.

10.1021/jp045516+ CCC: $30.25
Published on Web 01/20/2005

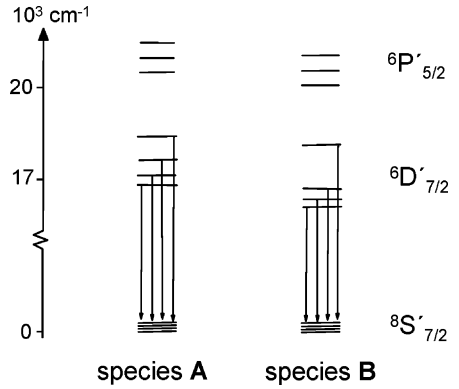

Figure 1. Graphical representation of the $^6D'_{7/2} \rightarrow {}^8S'_{7/2}$ photoemission of Cm^{3+}, showing the main transition occurring from the lowest $^6D'_{7/2}$ excited state level and the minor transitions from thermally populated second, third, and fourth levels for species **A** and **B** with different ligand fields.

300 °C,[23] and Yb^{3+} in dilute HNO_3 and HCl up to 500 °C.[24] Time-resolved laser fluorescence spectroscopy (TRLFS) has also been used to study some luminescence properties of Sm^{3+}, Eu^{3+}, Tb^{3+}, and Dy^{3+} in aqueous H_2O and D_2O solutions up to 230 °C.[25]

The present paper addresses the temperature dependency of An^{3+} hydration exemplified by the Cm^{3+} aqua ion, using TRLFS. TRLFS is a versatile tool for the quantification of Cm^{3+} species at trace level concentration in aqueous media because of its high emission yield and good selectivity.[26,27] The spectra results from the emission of the lowest excited $^6D'_{7/2}$ state to the ground $^8S'_{7/2}$ state. Both levels are split by the ligand field into four Kramers doublets. While the splitting of $^6D'_{7/2}$ may be several hundred wavenumbers, the splitting of $^8S'_{7/2}$ is an order of magnitude smaller and is normally not resolved. For a Cm^{3+} aqua ion (**A**) a single electronic transition from the lowest $^6D'_{7/2}$ crystal field level and additional hot bands from thermally populated higher crystal field levels are expected, while for a species (**B**) with stronger ligand field a red-shifted spectrum is expected; see Figure 1.

To study the possible transition from a nona- to an octahydrated Cm^{3+}, emission spectra are measured between 20 and 200 °C in dilute aqueous perchloric acid to prevent hydrolysis and electrolyte medium anion complexation. In support of interpretation reference is made to nona- and octahydrated crystalline data. This is provided by incorporation of Cm^{3+} in the crystalline hosts $[La(H_2O)_9]Cl_3 \cdot 15\text{-crown-}5 \cdot H_2O$ (**1**) and $[Y(H_2O)_8]Cl_3 \cdot 15\text{-crown-}5$ (**2**), in which the hydrated rare-earth/Cm^{3+} entities exhibit distorted tri- and bicapped trigonal prismatic coordination geometries, respectively.[28,29]

2. Experimental Section

2.1. Crystalline Host Compounds. The preparation of $[La(H_2O)_9]Cl_3 \cdot 15\text{-crown-}5 \cdot H_2O$ (**1**) and $[Y(H_2O)_8]Cl_3 \cdot 15\text{-crown-}5$ (**2**) followed schemes described in detail elsewhere.[28,29] High purity (99.99%) La_2O_3 and Y_2O_3 were used to prevent emission from impurity ions. The oxides were dissolved in dilute hydrochloric acid by heating and stirring. Traces of Cm^{3+}(aq) were introduced to these solutions, followed by addition of 15-crown-5 (1 equiv mol dissolved in acetonitrile−methanol 1:3). Large (∼1−5 mm), colorless crystals of **1** and **2** were formed after slow evaporation of the water solvent at room temperature. The La^{3+} and Y^{3+} content of **1** and **2** was determined by EDTA titration, using xylene orange as an indicator,[30] while the chloride content was determined by cation exchange (Dowex 50W-X8, H^+-form), followed by standard acid−base titrations. The crystal structures of **1** and **2** were determined with single-crystal X-ray diffraction methods. The structure of **1** is not reported before but is isomorphous with that of Nd,[28] and **2** is identical with the previously published structure.[29]

TABLE 1: Observed $^6D'_{7/2}$ Crystal Field Energy Levels from Emission Spectra of Hydrated Cm^{3+} in 1 and 2 and Aqueous Solution at 20 and 200 °C

sample	E/cm^{-1}	ΔE/cm^{-1}	assign[a]
$[Cm(H_2O)_9]^{3+}$ in **1**	16 850	0	A_1
	16 940	90	A_2
	17 170	320	A_3
	17 390	540	A_4
$[Cm(H_2O)_8]^{3+}$ in **2**	16 742	0	B_1
	16 830	88	B_2
	16 942	200	B_3
	17 420	678	B_4
Cm^{3+}(aq), 20 °C	16 840	0	A_1
	16 900	60	A_2
Cm^{3+}(aq), 200 °C	16 735	0	B_1
difference spectrum	16 830	95	B_2[b]
	16 960	225	B_3[c]
	17 130	290[e]	A_3
	17 430	695	B_4[d]

[a] A_i and B_i are the assigned emission bands corresponding to the ith crystal field level of nona- and octahydrated species $[Cm(H_2O)_9]^{3+}$ (**A**) and $[Cm(H_2O)_8]^{3+}$ (**B**), respectively. [b] Band not resolved due to line broadening; peak position estimated from **2**. [c] Overlap between A_2 and B_3. [d] Overlap between A_4 and B_4. [e] $\Delta E = 17130(A_3) - 16840(A_1)$. Estimated errors: ±5, ±10, ±20, and ±20 cm^{-1} for bands corresponding to levels 1, 2, 3, and 4, respectively.

2.2. TRLFS. TRLFS was performed by using a setup described in detail elsewhere.[26] In brief, an excimer pumped dye laser system (Lamda Physics, EMG 201 and FL 30029), emitting at 375 nm (26 670 cm^{-1}) with a pulse energy of ca. 10 mJ at 10 Hz repetition rate, was used for excitation. Spectra were recorded by an optical multichannel analyzer, which consists of a polychromator (Jobin Yvon, HR 320) with a 1200 line mm^{-1} grating and a time-gateable intensified photodiode array with 1024 Si photodiodes (Spectroscopy Instruments, ST 180, IRY 700 G). To cover the total spectral range of the $^6D'_{7/2} \rightarrow {}^8S'_{7/2}$ transition from 560 to 630 nm, two overlapping spectra were recorded at each temperature with the central wavelength set at 580 and 610 nm. The obtained spectra were then merged to one spectrum.

For the discrimination of Rayleigh and Raman scattering a minimal time delay of 1.2 μs between laser pulse and camera gating was used. The gate width of the camera was set to 1 ms for H_2O and 10 ms for D_2O solutions. For lifetime measurements the delay time was scanned with time intervals of typically 5 and 25 μs for H_2O and D_2O solutions, respectively. The lifetime, τ, was obtained by fitting the integrated intensity (I) at time t after the laser pulse to

$$I(\lambda) = I_0(\lambda) \exp(-t/\tau) \qquad (2)$$

where I_0 is the intensity at $t = 0$. The emission decay was found to be monoexponential at each temperature.

For spectra deconvolution and fitting, spectra were transferred to the GRAMS32 software package (Galactic Industries Inc.), which gave the center, height, full width at half-maximum (fwhm), and the Gaussian−Lorentzian mixing for each of the four component bands. The bands A_1, A_2, B_1, and B_2, assigned in Table 1 and displayed in Figure 3, were found to be about 75% Lorentzian, whereas the A_3, A_4, B_3, and B_4 are nearly 100%

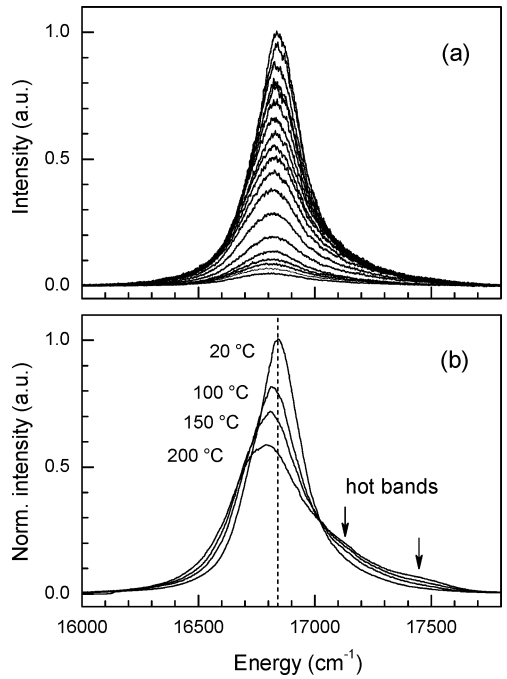

Figure 2. (a) ${}^6D'_{7/2} \rightarrow {}^8S'_{7/2}$ photoemission spectra of 0.5 μM Cm^{3+} in 0.1 M $HClO_4$ aqueous solution from 20 to 200 °C (from top to bottom) at saturated vapor pressure with an increment of 10 °C. (b) Normalized (peak area) spectra at 20, 100, 150, and 200 °C, showing a red shift ($\sim$100 cm^{-1}) and the appearance of two distinct shoulders at higher energy (due hot bands) at elevated temperature.

Gaussian. The peak heights were allowed to vary whereas the bandwidths were correlated such that fwhm($A_1 + A_2$) = fwhm-($B_1 + B_2$).

3. Results and Discussion

3.1. Temperature Influence on the Photoemission of the Cm^{3+} Aqua Ion. Figure 2a shows the influence of temperature on the photoemission spectra of Cm^{3+} in an acidified (0.1 M $HClO_4$) aqueous solution between 20 and 200 °C. In accordance with literature data,[27] the spectrum at room temperature (20 °C) shows a fairly symmetric band with a peak maximum at 16 840 cm^{-1} (593.8 nm) and fwhm $\sim$190 cm^{-1}. With increasing temperature the emission intensity decreases by a factor of almost ten, accompanied by an asymmetric broadening on the blue side and a peak shift to lower energy (red shift). These features are clearly seen in Figure 2b where spectra at selected temperatures are normalized to equal peak area. The two shoulders appearing at about 17 100 (585 nm) and 17 450 cm^{-1} (573 nm) in the spectra at elevated temperatures are recognized as hot bands.

The photoemission spectrum is a sensitive probe for the coordination environment of the Cm^{3+} ion. The observed red shift with increasing temperature thus indicates a strengthening of its ligand field. Various conceivable causes may be considered. The physical properties of water change considerably at elevated temperature, e.g., its relative permittivity and its autoionization, which to some extent may influence the curium−water interaction. The red shift is not caused by vibronic transitions, as the corresponding blue-shifted satellites are not observed in the spectra (vibronic coupling gives rise to line broadening). Hydrolysis and inner-sphere complexation with perchlorate ions are expected to induce a red shift. However, hydrolysis of Cm^{3+}(aq) is not significant at pH $\ll$ 6.0 (β_{11} = 6.7 at 20 °C),[27] and ClO_4^- is also a weak ligand and does not form inner-sphere complexes.[31] The formation of hydroxide and perchlorate complexes at elevated temperatures can be excluded, because the emission spectra at different $HClO_4$ concentrations (10^{-3} to 7 M) showed no measurable variation between 20 and 200 °C (spectra not shown), even after several heating and cooling cycles. We therefore attribute the bathochromic shift at elevated temperature to a Cm^{3+} aqua species with different local structure than at room temperature.

A temperature-dependent equilibrium between $[Cm(H_2O)_9]^{3+}$ (**A**) and $[Cm(H_2O)_8]^{3+}$ (**B**) with entropy driven preference for species **B** with increasing temperature, cf. eq 1, can explain the observed spectral behavior. Each spectrum at a given temperature is then a superposition of the individual spectra of **A** and **B**. The rather symmetric band at room temperature shows a predominance of **A** with only a small but significant shoulder at 16 742 cm^{-1}, representing species **B**. The red-shifted band at 200 °C shows the presence of a significant amount of **B** emitting at lower energy. An estimate for the pure spectrum of **B** may be obtained by means of a "difference spectrum", i.e., by subtracting an appropriate amount ($\sim$1/3) of the room-temperature spectrum from that at 200 °C.

Figure 3 shows the emission spectra of the aqueous solution at 20 °C and the difference spectrum at 200 °C, in comparison with the room-temperature spectra of the $[Cm(H_2O)_9]^{3+}$ and $[Cm(H_2O)_8]^{3+}$ species in the crystalline host compounds **1** and **2**. Each spectrum is deconvoluted with component bands (see Experimental Section) corresponding to electronic transitions of the thermally populated ${}^6D'_{7/2}$ crystal field levels level to the ground state. The spectra of **1** and the aqueous solution at 20 °C are rather similar with almost identical peak positions. The former is dominated by two bands at 16 850 (593.5 nm) (A_1) and 16 940 cm^{-1} (590.3 nm) (A_2) with approximately a Boltzmann intensity ratio, corresponding to the emission from the first and second ${}^6D'_{7/2}$ energy levels. The low-intensity band at 17 170 cm^{-1} (582.4 nm) (A_3) is assigned to the third crystal field level. In the spectrum of Cm^{3+}(aq) at 20 °C the A_1 and A_2 components are not resolved; however, in a frozen solution of Cm^{3+} in 0.1 M $HClO_4$ at 130 K a hot band appears at about 16 900 cm^{-1} (A_2).[21b] Contrary to the crystalline compound **1**, however, a pronounced shoulder is seen at the red side, which is accounted for by an additional component band (B_1). The position of this band, 16 742 cm^{-1} (597.3 nm), is in full agreement with that of B_1 in the spectrum of $[Cm(H_2O)_8]^{3+}$ in **2**. Here, B_2 and B_3 are also identified, and B_4 is observed as a weak feature at higher energy. In the difference spectrum, B_1 and B_2 are not resolved due to line broadening and are combined, while the shoulders at higher energy are fitted with three bands assigned to B_3, A_3, and $A_4 + B_4$, cf. Figure 3 and Table 1.

A clear separation of the contributions of **A** and **B** to the emission spectra is not feasible. To quantify their contribution to the spectra, some simplifications must be made in the fitting procedure. As the components A_2 and B_2 cannot be resolved from those of A_1 and B_1, they are combined to $A_1 + A_2$ and $B_1 + B_2$, and since the third and fourth hot bands of **A** and **B** overlap they are represented by two bands to account for the asymmetry at higher energy, but are not included in the quantification. The fitted spectra at selected temperatures are presented in Figure 4.

The relative concentration of **A** and **B** may be obtained from the integrated intensities of their corresponding emission bands ($A_1 + A_2$ and $B_1 + B_2$) according to

$$[\mathbf{B}] = I_{\mathbf{B}}/(F_{\mathbf{B}}I_{\mathbf{A}} + I_{\mathbf{B}}); \text{ and } [\mathbf{A}] = 1 - [\mathbf{B}] \qquad (3)$$

where the emission intensity factor $F_{\mathbf{B}}$ accounts for the different

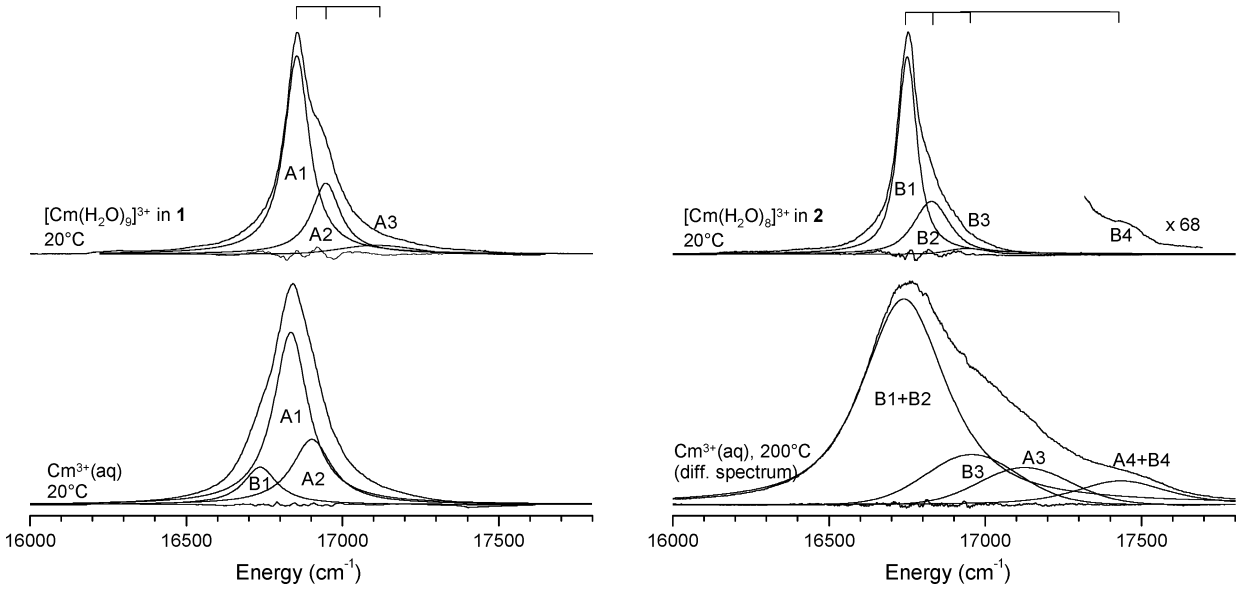

Figure 3. Comparison, peak deconvolution, and assignments of component bands of ${}^6D'_{7/2} \rightarrow {}^8S'_{7/2}$ emission spectra of hydrated Cm^{3+} in **1** and **2** and aqueous solution at 20 and 200 °C (difference spectrum). Each spectrum is deconvoluted and fitted with component bands corresponding to the emission contribution from the thermally populated ${}^6D'_{7/2}$ levels. The bands are denoted A_1-A_4 and B_1-B_4 for assigned $[Cm(H_2O)_9]^{3+}$ (**A**) and $[Cm(H_2O)_8]^{3+}$ (**B**) species, respectively. In the difference spectrum, the second hot bands of **A** and **B** species (A_3 and B_3) are of similar magnitude. Residuals of the fits to the experimental spectra are shown.

absorptivity and quantum yield of species **B** with respect to **A** ($F_{\mathbf{A}} = 1$). The crystal field strength of the water ligand in f-element complexes is considered to be weak and comparable to that of Cl^-.[32] Crystal field effects are therefore small for species **A** and **B**, which is reflected in the relatively small difference between their peak maxima of the emission spectra. No major changes of the peak maximum or transition probability are to be expected for the excitation band. Moreover, the observed emission intensities are averaged over transitions between the two lowest populated crystal field levels of the ${}^6D'_{7/2}$ state and all the crystal field levels of the ground state. Therefore, changes in coordination symmetry of **A** and **B** will probably have minor effects on the quantum yield. As will be discussed below, the nonradiative decay rate is dominated by the number of coordinated water molecules and should therefore be about 10% smaller in **B** compared to **A**. For these reasons the emission intensity factors are expected to be very similar for **A** and **B**. In accordance with intensity factors found for various Cm^{3+} complexes without ligand sensitized emission, $F_{\mathbf{B}}$ is estimated to be in the range 0.7−1.5. In the following, $F_{\mathbf{B}} = 1$ is assumed; however, consequences of the variation of $F_{\mathbf{B}}$ on the derived thermodynamic parameters will also be discussed.

Figure 5 (left) shows that [**A**] decreases from ca. 0.9 at room temperature to approximately 0.6 at 200 °C. The thermodynamic parameters $\Delta H°$ and $\Delta S°$ associated with eq 1 are obtained from the Van't Hoff equation

$$-\ln K = \Delta G°/RT = \Delta H°/RT - \Delta S°/R \qquad (4)$$

by plotting $-\ln K$ against $1/T$, where $K(T)$ is the temperature-dependent equilibrium constant defined as $K(T) = [\mathbf{B}]/[\mathbf{A}]$, which assumes that the water activity is approximately constant with temperature and that the ratio of the activity coefficient of **A** and **B** is temperature independent. Linear regression through the data points in Figure 5 (right) yields $\Delta H° = +13.1 \pm 0.4$ kJ mol^{-1} and $\Delta S° = +25.4 \pm 1.2$ J mol^{-1} K^{-1}, which corresponds to $\Delta G^{298} = +5.5 \pm 0.6$ kJ mol^{-1} and $K^{298} = 0.11 \pm 0.02$. By including a variation in the temperature-independent $F_{\mathbf{B}}$ between 0.7 and 1.5, $\Delta S°$ will vary between 21.9 and 28.7

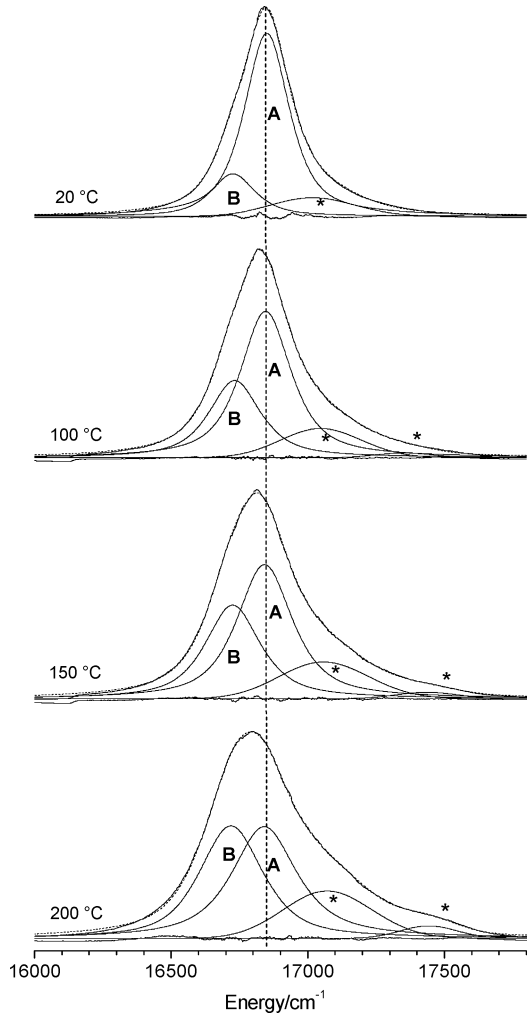

Figure 4. Examples of curve fitting of emission spectra of Cm^{3+}(aq) at 20, 100, 150, and 200 °C, deconvoluted into **A** and **B** species and their combined hot bands ("*"). Experimental data, individual fitted component bands and residuals, are shown with solid lines and fits to the data are shown with dashed lines.

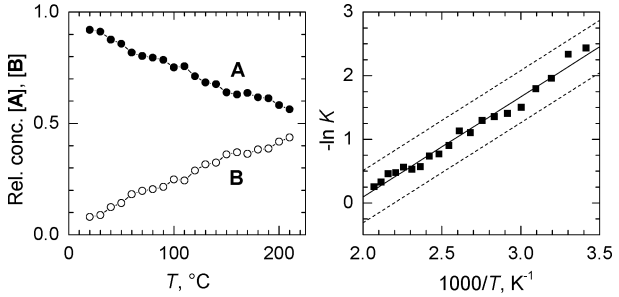

Figure 5. (Left) Relative concentration of species **A** and **B** as function of temperature, assuming that $F_B = F_A = 1$. (Right) Van't Hoff linear representation $-\ln K$ versus $1/T$. Linear regression yields $\Delta H = 13.1 \pm 0.4$ kJ mol^{-1} and $\Delta S = 25.4 \pm 1.2$ J mol^{-1} K^{-1}. The upper and the lower dashed lines correspond to values for $-\ln K$ where $F_B = 0.7$ and 1.5, respectively.

TABLE 2: Thermodynamic Data Associated with $[M(H_2O)_9]^{3+} \rightarrow [M(H_2O)_8]^{3+} + H_2O$ from Variable-Temperature and Variable-Pressure Studies[a]

	Ce^{3+}(aq)	Cm^{3+}(aq)[c]
$\Delta H°$/kJ mol^{-1}	+13[b]	+13.1 ± 0.4
$\Delta S°$/J mol^{-1} K^{-1}	+33[b]	+25.4 ± 1.2
$\Delta V°$/cm^3 mol^{-1}	+10.9 ± 0.3[c]	
$K(298)$[d]	0.28;[b] 0.21 ± 0.03[c]	0.11 ± 0.02

[a] This work; the data are derived assuming $F_B = F_A$, see text and Figure 5. [b] Reference 36. [c] Reference 37. [d] $K(298) = \{[M(H_2O)_8]^{3+}\}/\{[M(H_2O)_9]^{3+}\}$.

J mol^{-1} K^{-1}, whereas $\Delta H°$ is unaltered. The corresponding $-\ln K$ values are represented by two dashed lines in Figure 5, giving a maximum variation in [**B**] between 0.07 and 0.14 at 298 K.

There are only a few spectroscopic studies that have given direct evidence for an equilibrium between $[Ln(H_2O)_9]^{3+}$ and $[Ln(H_2O)_8]^{3+}$ ions in aqueous solution. Recently, $^5D_1 \leftarrow {}^7F_0$ excitation and $^5D_0 \rightarrow {}^7F_{1,2}$ emission spectra of 0.1 M $EuCl_3$-(aq) were evaluated and compared to the spectra of crystalline $[Eu(H_2O)_9](BrO_3)_3$, $[Eu(H_2O)_9](C_2H_5SO_4)_3$, and $[Eu(H_2O)_8][(V_{10}O_{28})]\cdot 8H_2O$, and it was concluded that about 70% of the hydrated Eu^{3+} ions are present as octaaqua species in aqueous solution at room temperature.[33] In the 5d ← 4f UV−vis absorption of Ce^{3+}(aq) a weak sixth band appears at 295 nm. Since a single aqua species would give rise to a maximum of five Kramers doublets, the appearance of this additional band was attributed to the occurrence of a minor quantity of an octahydrated ion species.[34,35] This assignment was supported by comparison with the spectrum of Ce^{3+} in $[La(H_2O)_9](C_2H_5SO_4)_3$.[35] It was found that the 295 nm band increases with temperature and decreases with pressure, indicating a T−P dependent equilibrium between nona- and octahydrated Ce^{3+} ions.[36,37] The thermodynamic parameters obtained from these studies are given in Table 2 together with those of Cm^{3+}.

It is noteworthy that the equilibrium constant, $K(T)$, at ambient T−P conditions is found to be higher for Ce^{3+} than for Cm^{3+} (cf. Table 2) despite their different ionic radii, $r(Ce^{3+}) = 1.143$ Å and $r(Cm^{3+}) = 1.094$ Å.[38,39] However, in both studies comparable values of ΔS are obtained, +33 J and +25 mol^{-1} K^{-1} for Ce^{3+} and Cm^{3+}, respectively. It is reasonable that ΔS is positive and relatively large as it includes the entropy change of a dissociation of a water ligand to the aqueous bulk. Moreover, these values are comparable to the melting entropy of ice, about +25 J mol^{-1} K^{-1}.[40] Further support for an equilibrium between nona- and octahydrated Ln^{3+} ions in the middle of the lanthanide series comes from variable-temperature and variable-pressure ^{17}O NMR studies on water exchange on Ln^{3+} aqua ions.[41,42] The fact that the intermediate ions exhibit the fastest water exchange rates correlates with the relatively small energy difference between the octa- and nonaaqua ions.[3b]

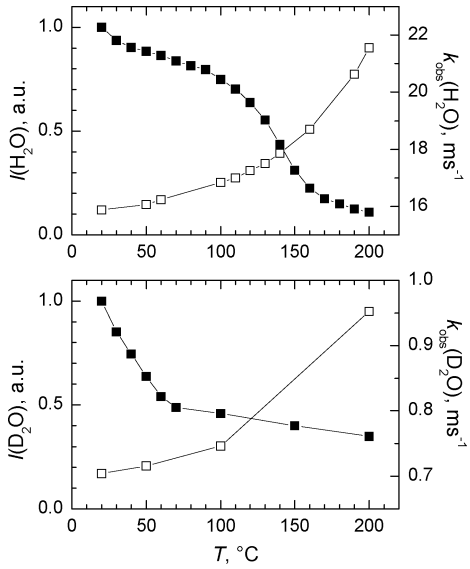

Figure 6. Normalized emission intensities, I (■), and emission decay rate constants, k_{obs} (=$1/\tau$) (□), of hydrated Cm^{3+} in H_2O and D_2O as a function of temperature.

3.2. Temperature-Dependent Emission Intensities and Lifetimes of the Cm^{3+} Aqua Ion. Figure 6 shows the temperature dependence of the emission intensity, I, and the observed decay rate, k_{obs} (corresponding to the reciprocal lifetime, τ^{-1}), of the emitting $^6D'_{7/2}$ energy level for hydrated Cm^{3+} in H_2O and D_2O between 20 and 200 °C. The general trend of the temperature dependency of these quantities is similar for both solvents. The intensity decreases by a factor of about 10 and the lifetime decreases by one-third. In H_2O the strongest change of the emission intensity with temperature is found in the intermediate region ~100−150 °C, with somewhat lower dependencies at higher and lower temperatures. The lifetime changes relatively little at lower temperature but the dependency becomes stronger with increasing temperature. This shows that there is no simple relationship between the emission intensity and lifetime for such an extended temperature range, neither in H_2O nor in D_2O.

In H_2O at room temperature the lifetime is determined to be 64 ± 3 μs and in D_2O 1370 ± 30 μs, whereas at 200 °C the lifetime is 42 ± 4 μs in H_2O and 1050 ± 50 μs in D_2O. Previously reported values at ambient temperature are comparable, 65 and 1270 μs in H_2O and D_2O, respectively.[43] However, the latter value is somewhat lower than in the present study, which may be due to impurity with H_2O in the previous study.

The considerable difference in lifetimes in H_2O and D_2O is associated with the much higher transition probability from excited Cm^{3+} to overtones of OH vibrations of coordinated water molecules than to the corresponding OD overtones. For several hydrated lanthanide ions, e.g., Eu^{3+}, Tb^{3+},[44] and Cm^{3+},[43,4a] it is established that the emission decay rate can be expressed as

$$k_{obs} = k_r + k_{nr} + n \cdot k_{H_2O} \quad (5)$$

where k_r is the radiative decay rate constant, k_{nr} is the nonradiative decay rate constant, which includes quenching processes other than that of coordinated water, k_{H_2O} is the decay rate constant for one coordinated water molecule, and n is the number of coordinated water molecules. The radiative lifetime has been calculated to be ~1.3 ms for the Cm^{3+} aqua ion.[45] In

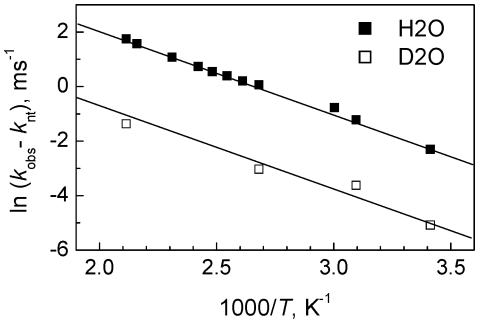

Figure 7. $-\ln(k_{obs} - k_{nt})$ versus $1/T$ (Arrhenius plot) of data in Figure 6. Solid lines = fits to eq 7, $k_{obs} = k_{nt} + A \exp(-\Delta E/RT)$.

the present study the lifetime is obtained as 1.37 ms in D_2O at room temperature. Since k_r and k_{nr} are basically the same for H_2O and D_2O, and $k_{D_2O} \ll k_{H_2O}$, n may be expressed as

$$n = (k_{obs}(H_2O) - k_{obs}(D_2O))/k_{H_2O} \quad (6)$$

This linear relation between the hydration number and the decay rate was first derived for Eu^{3+} and Tb^{3+} ions for two series of crystalline rare-earth hydrates with known structures.[44] Subsequently, a simplified version of eq 6 was applied for Cm^{3+}, where $n = 0.65k_{obs} - 0.88$.[43] This corresponds to $k_{H_2O} = 1.54$ ms^{-1} in eq 6 and $k_{obs}(D_2O) = 1.35$ ms^{-1}, the latter of which is assumed to be small and constant in all deuterated systems. These values may be compared to those derived from eq 6 in the present study, $k_{H_2O} = 1.66$ ms^{-1}, by assuming $n = 9$ at 20 °C and $k_{obs}(D_2O) = 0.73$ ms^{-1}. Based on these parameters, an increase of the hydration number from 9.0 at room temperature to about 13.8 at 200 °C is calculated, which is similar to the result obtained by using the equation from ref 43. The calculated increase of the hydration number with temperature is not realistic and indicates that k_{H_2O} must be temperature dependent.

In general, radiative relaxation shows little temperature dependency whereas nonradiative processes often involve population of higher electronic or vibronic levels, which necessitates temperature-dependent activation energy. Figure 7 shows the observed decay rates of Cm^{3+} in H_2O and D_2O, plotted on a logarithmic scale against $1/T$ (Arrhenius plot). The lines show fitting of the experimental data to

$$k_{obs} = k_{nt} + A \exp(-\Delta E/RT) \quad (7)$$

where k_{nt} contains the temperature-independent decay processes, A is the frequency factor and ΔE is the activation energy of the decay process. The ratio found for $k_{obs}(H_2O)/k_{obs}(D_2O) = 22.7$ is very similar to that of $A(H_2O)/A(D_2O)$, yielding $A = 5.2 \times 10^6$ and 2.3×10^5 s^{-1} for H_2O and D_2O, respectively. The obtained activation energy is approximately the same in H_2O and D_2O, about 26.5 kJ mol^{-1} (2250 cm^{-1}), indicating a similar temperature-dependent quenching mechanism of the $^6D'_{7/2}$ state for hydrated Cm^{3+} in H_2O and D_2O. From the absorption spectrum of Cm^{3+} in 1 M $HClO_4$ the energy difference between the first and second excited-state levels, $^6D'_{7/2}$ and $^6P'_{5/2}$, was obtained as 3255 cm^{-1}.[45] The calculated activation energy deduced from eq 7 is lower than the measured energy difference between the lowest fluorescent and next higher state, 2250 cm^{-1} compared to 3255 cm^{-1} (at room temperature); cf. Figure 1. Quenching through thermal population of the $^6P'_{5/2}$ level is therefore feasible, though it imposes an extremely short lifetime of $^6P'_{5/2}$ as only a small fraction is populated (e.g., $\sim 5.1 \times 10^{-5}$ at 200 °C).

A previous study on the temperature dependency of the radiationless decay of the $^5D_0$ level for Eu^{3+} in D_2O showed that the activation energy was slightly higher than but close to $\sim$1700 cm^{-1}, the energy gap between the $^5D_0$ and $^5D_1$ levels, and that the lifetime of $^5D_1$ was about 10^{-2} to 10^{-4} shorter than to that of $^5D_0$ for Eu^{3+} in H_2O solution.[46] This indicates that the decrease in lifetime at elevated temperature can be attributed to the thermal population of the $^5D_1$ level, which is very short lived. In a recent variable-temperature TRLFS study of Eu^{3+} and Tb^{3+} in H_2O and D_2O from 20 to 230 °C, it was established that both the emission intensity and lifetime decrease significantly with increasing temperature; however, remarkably small activation energies were derived.[25]

The emission lifetimes (at 20 °C) of the $[Cm(H_2O)_9]^{3+}$ and $[Cm(H_2O)_8]^{3+}$species in **1** and in **2** are obtained as 74 ± 2 and 68 ± 2 μs, respectively. Because the nonradiative decay is primarily determined by the number of water ligands (cf. eq 6) it may seem odd that the lifetime is shorter for the octahydrate than for the nonahydrate. However, considering that the mean Cm−O bond distance is shorter in the octahydrate, the energy transfer to the water ligand becomes more efficient and, consequently, the lifetime is shorter. Similarly, the contraction of the coordination shell expected for the Cm^{3+} aqua ion at elevated temperature may shorten the lifetime.

4. Conclusions

This paper presents the first variable-temperature study (20−200 °C) of the hydrated Cm^{3+} ion by time-resolved laser fluorescence spectroscopy. The study shows that several of the spectroscopic quantities associated with the photoemission of the Cm^{3+} aqua ion are strongly temperature dependent. With increasing temperature these are (i) decrease in emission intensity, (ii) decrease in lifetime, (iii) appearance of a new redshifted band, and (iv) progressive appearance of hot bands.

The temperature dependency of the emission intensity lifetime may be related to different processes proposed for other comparable fluorescent ions, such as (i) progressive population of a next very short-lived level above the main fluorescent level and (ii) contraction of the coordination shell resulting in increasing transition probability.

In addition to the main emission band appearing at room temperature, an additional red-shifted band grows in with increasing temperature. By comparison with crystalline reference compounds incorporating $[Cm(H_2O)_9]^{3+}$ and $[Cm(H_2O)_8]^{3+}$ ions with defined coordination geometries, this new band may be associated to an octahydrated Cm^{3+} ion. However, the symmetry of the solution species cannot be unambiguously determined by this comparison. Furthermore, hot bands are related to these two different bands based on their energy difference and relative intensities compared to the respective main bands. Clarification of the actual processes involved requires further experimental work, including application of additional experimental methods, and strong interaction with quantum-chemical studies.

Acknowledgment. We thank G. Buckau and B. Schimmelpfennig for helpful comments and discussions.

Supporting Information Available: Raw data showing the time dependency of the emission decay of Cm^{3+}(aq) in H_2O at selected temperatures (Figure S1), molecular structures (from single-crystal XRD) showing the coordination polyhedra of the $[La(H_2O)_9]^{3+}$ and $[Y(H_2O)_8]^{3+}$ entities in the crystal hosts **1** and **2**, respectively (Figure S2), and a comparison between the emission spectra of the aqueous solution at 20 and 200 °C with

those of **1** and **2** (Figure S3). This material is available free of charge via the Internet at http://pubs.acs.org.

References and Notes

(1) Guillaumont, R.; Fanghanel, T.; Fuger, J.; Grenthe, I.; Neck, V.; Palmer, D. A.; Rand, M. H. *Update on the Chemical Thermodynamics of Uranium, Neptunium, Plutonium, Americium and Technetium*; NEA-TDB, Vol. 5; Mompean, F. J., Illemassene, M., Domenech-Orti, C., Ben Said, K., Eds.; Elsevier B.V.: Amsterdam, The Netherlands, 2003.

(2) Haas, J. R.; Shock E. L.; Sassani, D. C. *Geochim. Cosmochim. Acta* **1995**, *59*, 4329−4350.

(3) For recent reviews, see e.g.: (a) Ohtaki, H. *Monatsh. Chem.* **2001**, *132*, 1237. (b) Helm, L.; Merbach, A. E. *Coord. Chem. Rev.* **1999**, *187*, 151−181. Richens, D. T. *The Chemsitry of Aqua Ions*; Wiley: Chichester, U.K., 1997. (c) Lincoln, S. F.; Merbach, A. E. Substitution Reactions of Solvated Metal Ions. *Adv. Inorg. Chem.* **1995**, *42*, 2−88.

(4) (a) Billard, I. Lanthanide and Actinide Solution Chemistry Studied by Time-Resolved Laser-Induced Spectroscopy (TRLS). In *Handbook on the Physics and Chemistry of Rare Earths*; Gschneidner, K. A., Jr., Bünzli, J.-C., Pecharsky, V. K., Eds.; Elsevier: Amsterdam, The Netherlands, 2003; Vol. 33, Chapter 216. (b) Choppin, G. R.; Rizkalla, E. N. Solution Chemistry of Actinides and Lanthanides. In *Handbook on the Physics and Chemistry of Rare Earths. Lanthanides/Actinides*: *Chemistry*; Gschneidner, K. A., Jr., Eyring, L., Choppin, G. R., Lander, G. H., Eds.; Elsevier Science: Amsterdam, The Netherlands, 1994; Vol. 18, Chapter 128, pp 559−590.

(5) David, F. H.; Fourest, B. *New J. Chem.* **1997**, *21*, 167−176.

(6) David, F. H.; Vokhmin, V. *New J. Chem.* **2003**, *27*, 1627−1632.

(7) Rizkalla, E. N.; Choppin, G. R. Lanthanides and Actinides Hydration and Hydrolysis. In *Handbook on the Physics and Chemistry of Rare Earths. Lanthanides/Actinides*: *Chemistry*; Gschneidner, K. A., Jr., Eyring, L., Choppin, G. R., Lander, G. H., Eds.; Elsevier Science: Amsterdam, The Netherlands, 1994; Vol. 18, pp 529−558.

(8) Habenschuss, A.; Spedding, F. H. *J. Chem. Phys.* **1980**, *73*, 442−450.

(9) Helm, L.; Merbach, A. E. *Eur. J. Solid State Inorg. Chem.* **1991**, *28*, 245−250. Cossy, C.; Helm, L.; Powell, D. H.; Merbach, A. E. *New J. Chem.* **1995**, *19*, 27−35.

(10) Kowall, Th.; Foglia, F.; Helm, L.; Merbach, A. *J. Am. Chem. Soc.* **1995**, *117*, 3790−3799.

(11) Floris, F. M.; Tani, A. *J. Chem. Phys.* **2001**, *115*, 4750−4765.

(12) David, F.; Revel, R.; Fourest, B.; Hubert, S.; Le Du, J. F.; Den Auwer, C.; Madic, C.; Morss, L. R.; Ionova, G.; Mikhalko, V.; Vokhmin, V.; Nikonov, M.; Berthet, J. C.; Ephritikhine, M. In *Speciation, Techniques and Facilities for Radioactive Materials at Synchrotron Light Sources*; Nuclear Energy Agency: Organisation for Economic Co−Operation and Development: Grenoble, France, 1998; pp 95−100.

(13) Antonio, M. R.; Soderholm, L.; Williams, C. W.; Blaudeau, J.-P.; Bursten, B. E. *Radiochim. Acta* **2001**, *89*, 17−25.

(14) Allen, P. G.; Bucher, J. J.; Shuh, D. K.; Edelstein, N. M.; Reich, T. *Inorg. Chem.* **1997**, *36*, 4676−4683.

(15) Allen, P. G.; Bucher, J. J.; Shuh, D. K.; Edelstein, N. M.; Craig, I. *Inorg. Chem.* **2000**, *39*, 595−601.

(16) Reich, T.; Geipel, G.; Funke, H.; Hennig, C.; Rossberg, A.; Bernhard, G. In *FZR-285, Annual Report 1999*; Bernhard, G., Ed.; Forschungszentrum Rossendorf, Institute of Radiochemistry: Rossendorf, Germany, 2000; p 72.

(17) Conradson, S. D. *Appl. Spectrosc.* **1998**, *252A*, 52.

(18) Stumpf, T.; Funke, H.; Hennig, C.; Rossberg, A.; Reich, T.; Fanghänel, T. In *FZR-373, Annual Report 2002*; Bernhard, G., Ed.: Forschungszentrum Rossendorf, Institute of Radiochemistry: Rossendorf, Germany, 2003; p 1.

(19) Antonio, M. R.; Williams, C. W.; Soderholm, L. *Radiochim. Acta* **2002**, *90*, 851−856.

(20) Revel, R.; Auwer, C. Den; Madic, C.; David, F.; Fourest, B.; Hubert, S.; Le Du, J.-F.; Morss, L. R. *Inorg. Chem.* **1999**, *38*, 4139−4144.

(21) (a) Lindqvist-Reis, P.; Klenze, R.; Denecke, M. A.; Fanghänel, T.; Eichhöfer, A. To be submitted. (b) Rabung, T. Unpublished results.

(22) Migdisov, A. A.; Williams-Jones, A. E. *Geochim. Cosmochim. Acta* **2003**, *118*, 719−727.

(23) Anderson, A. J.; Jayanetti, S.; Mayanovic, R. A.; Bassett, W. A.; Chou, I.-M. *Am. Mineral.* **2002**, *87*, 262−268.

(24) Mayanovic, R. A.; Jayanetti, S.; Anderson, A. J.; Bassett, W. A.; Chou, I.-M. *J. Phys. Chem. A* **2002**, *106*, 6591−6599.

(25) Kimura, T.; Nagaishi, R.; Ariska, M.; Ozaki, T.; Yoshida, Z. *Radiochim. Acta* **2002**, *90*, 715−719.

(26) Chung, K. H.; Klenze, R.; Park, K. K.; Paviet-Hartmann, P.; Kim, J. I. *Radiochim. Acta* **1998**, *82*, 215−219.

(27) Wimmer, H.; Klenze, R.; Kim, J. I. *Radiochim. Acta* **1992**, *56*, 79−83.

(28) Rogers, R. D. *Inorg. Chim. Acta* **1988**, *149*, 307−314.

(29) Rogers, R. D.; Kurihara, L. K. *Inorg. Chim. Acta* **1986**, *116*, 171−177. Rogers, R. D.; Kurihara, L. K. *Inorg. Chim. Acta* **1987**, *129*, 277−282.

(30) Schwarzenbach, G.; Flaschka, H. *Die Komplexometrische Titration*; Ferdinand Enke: Stuttgart, Germany, 1965.

(31) To our knowledge there are no spectroscopic evidence for Ln(III)-ClO_4 or An(III)-ClO_4 species in aqueous solution below 8 M ClO_4^-. We have shown (results not yet published) that the room temperature Cm^{3+}-(aq) emission spectrum does not change with addition of $HClO_4$ up to 8 M.

(32) Carnal, W. T. *J. Less-Common Met.* **1989**, *156*, 221−235.

(33) Tilkens, L.; Randall, K.; Sun, J.; Berry, M. T.; May, P. S.; Yamase, T. *J Phys. Chem. A* **2004**, *108*, 6624−6628.

(34) Jørgensen, C. K.; Brinen, J. S. *Mol. Phys.* **1963**, *6*, 629−631.

(35) (a) Kaizu, Y.; Miyakawa, K.; Okada, K.; Kobayashi, H.; Sumitani, M.; Yoshihara, K. *J. Am. Chem. Soc.* **1985**, *107*, 2622−2626. (b) Okada, K.; Kaizu, Y.; Kobayashi, H.; Tanaka, K.; Marumo, F. *Mol. Phys.* **1985**, *54*, 1293−1306.

(36) Miyakawa, K.; Kaizu, Y.; Kobayashi, H. *J. Chem. Soc., Faraday Trans. 1* **1988**, *84*, 1517−1529.

(37) Laurenczy, G.; Merbach, A. E. *Helv. Chim. Acta* **1988**, *71*, 1971−1973.

(38) Shannon, R. D. *Acta Crystallogr.* **1976**, *A32*, 751−767.

(39) David, F. *J. Less-Common Met.* **1986**, *121*, 29.

(40) See, e.g.: Burgess, J. *Metal Ions in Solution*; Ellis Horwood: Chichester, U.K., 1978; Chapter 4.

(41) Cossy, C.; Helm, L.; Merbach, A. E. *Inorg. Chem.* **1988**, *27*, 1973−1979.

(42) Cossy, C.; Helm, L.; Merbach, A. E. *Inorg. Chem.* **1989**, *28*, 2699−2703.

(43) Kimura, T.; Choppin, G. R. *J. Alloys Compd.* **1994**, *213/214*, 313−317.

(44) Horrocks, W. DeW.; Sudnick, D. R. *J. Am. Chem. Soc.* **1979**, *101*, 334−340.

(45) Carnal, W. T.; Rajnak, K. *J. Chem. Phys.* **1975**, *63*, 3510−3514.

(46) Kropp, J. L.; Dawson, W. R. *J. Chem Phys.* **1966**, *45*, 2419−2420.